Two- and three-particle nonflow contributions to the chiral magnetic effect measurement by spectator and participant planes in relativistic heavy ion collisions

Yicheng Feng [1,*] Jie Zhao [1,†] Hanlin Li [2,‡] Hao-jie Xu [3,§] and Fuqiang Wang [1,3,‖]

[1]*Department of Physics and Astronomy, Purdue University, West Lafayette, Indiana 47907, USA*
[2]*College of Science, Wuhan University of Science and Technology, Wuhan, Hubei 430065, China*
[3]*School of Science, Huzhou University, Huzhou, Zhejiang 313000, China*

(Received 10 July 2021; accepted 15 February 2022; published 28 February 2022)

Correlation measurements with respect to the spectator and participant planes in relativistic heavy ion collisions were proposed to extract the chiral magnetic effect (CME) from background dominated azimuthal correlators. This paper investigates the effects of two- and three-particle nonflow correlations on the extracted CME signal fraction, $f_{\rm CME}$. It is found, guided by a multiphase transport (AMPT) model and the heavy ion jet interaction generator (HIJING) together with experimental data, that the nonflow effects amount to approximately $(4 \pm 5)\%$ and $(-5 \pm 3)\%$ without and with pseudorapidity gaps, respectively, in 20–50% centrality Au+Au collisions at $\sqrt{s_{NN}} = 200$ GeV.

DOI: 10.1103/PhysRevC.105.024913

I. INTRODUCTION

In quantum chromodynamics (QCD) vacuum, topological charge fluctuations can cause chiral anomaly in local domains, which violates the $\mathcal{CP}$ symmetry [1–5]. Because the spin of quarks is either parallel or antiparallel to a strong magnetic field depending on their charge, such a chiral anomaly would result in charge separation along the magnetic field. This is called the chiral magnetic effect (CME) [3–5]. In noncentral heavy ion collisions, the overlap participant zone allows the formation of metastable topological domains, whereas the spectator protons can provide an intense, transient magnetic field perpendicular on average to the reaction plane (RP, spanned by the impact parameter and beam directions) [4,6,7]. Thus, the CME is expected in relativistic heavy ion collisions, and, if measured, would be strong evidence for local $\mathcal{CP}$ violation in QCD [8].

Charge-dependent azimuthal correlators [9] are used to measure the CME-induced charge separation, $\Delta\gamma = \gamma_{\rm OS} - \gamma_{\rm SS}$, where

$$\gamma_{\alpha\beta} = \langle \cos(\phi_\alpha + \phi_\beta - 2\Psi_{\rm RP}) \rangle, \tag{1}$$

ϕ is the azimuthal angle of particle of interest (POI), the subscripts α, β indicate charge signs (OS for opposite-sign and SS for same-sign pairs) of two different particles, and $\Psi_{\rm RP}$ is the RP azimuthal angle. Strong positive $\Delta\gamma$ signals have been observed in both large collision systems (Au+Au at RHIC [10–13] and Pb+Pb at the LHC [14–18]) and small systems (d+Au at RHIC [19] and p+Pb at the LHC [15,16]). No CME signal is expected in the latter, indicating large background contaminations in $\Delta\gamma$. The backgrounds are caused by two-particle (2p) nonflow correlations, such as resonance decays, coupled with elliptic flow (v_2) of the correlated pairs [9,20–24]. It can be expressed as

$$\Delta\gamma_{\rm bkgd} = \frac{N_{\rm 2p}}{N^2} \langle \cos(\phi_\alpha + \phi_\beta - 2\phi_{\rm 2p}) \rangle v_{2,\rm 2p}, \tag{2}$$

where N is the POI multiplicity of a single charge ($N \approx N_+ \approx N_-$), $N_{\rm 2p}$ is the number of correlated pairs (such as the parent resonances), $\phi_{\rm 2p}$ is the azimuthal angle of the parent, and $v_{2,\rm 2p}$ is its elliptic flow with respect to (w.r.t.) RP, $v_{2,\rm 2p} = \langle \cos 2(\phi_{\rm 2p} - \Psi_{\rm RP}) \rangle$. Note that Eq. (2) refers to the difference between OS and SS (i.e., *charge dependent*); the sign-independent effects are already canceled. This background is a combined effect of 2p nonflow correlations and flow, and is customarily called "flow-induced" background.

To suppress the backgrounds, many techniques have been exploited, such as event shape engineering [16,17,25,26] and differential measurements in invariant mass [27,28]. These studies indicate that the backgrounds are dominant and the possible CME signal is consistent with zero. Recently, a new method [29,30] was invented to extract the CME signal by comparing $\Delta\gamma$ and v_2 w.r.t. two *different* planes [instead of the unmeasurable RP in Eq. (1)]: the participant plane (PP, reconstructed from produced particles) and the spectator plane (SP, reconstructed from spectators). We refer to the method as the SP/PP method. The method is, arguably, the most robust one on market as it measures two quantities in the *same* event which contain different amounts of the CME signal and background. It would give a rather robust measure of the CME if there were no nonflow contaminations. Such measurements have been performed by the STAR Collaboration [31,32]. The

*feng216@purdue.edu
†zhao656@purdue.edu
‡lihl@wust.edu.cn
§haojiexu@zjhu.edu.cn
‖fqwang@purdue.edu

purpose of this paper is to investigate the effects of nonflow contaminations on the extracted CME signal.

The rest of the paper is organized as follows. Section II recaps the SP/PP method and introduces a notation scheme to signal quantities that are affected by nonflow. Section III describes the nonflow contaminations to v_2^* and $\Delta\gamma^*$ (or C_3^*). Section IV presents model simulation results by a multiphase transport (AMPT) model and the heavy ion jet interaction generator (HIJING), respectively. Section V makes quantitative estimations of nonflow contributions to the $f_{\rm CME}^*$ in real data analysis by combining AMPT and HIJING simulation results together with inputs from experimental data. Section VI summarizes our work and gives a brief outlook.

II. METHODOLOGY

The SP/PP method [30] is rather straightforward. It exploits fluctuations in the collision geometry [33,34] that yields a nonunity $a \equiv \langle \cos 2(\Psi_{\rm PP} - \Psi_{\rm SP})\rangle$. Since the CME backgrounds are induced by v_2 of particles in the participant zone, $\Delta\gamma$ w.r.t. PP should contain the maximal background. As the background strength is proportional to v_2 [see Eq. (2)], it is reduced by the factor of a along the SP. On the other hand, since the CME signal is along the magnetic field created mainly by the spectator protons, $\Delta\gamma$ w.r.t. SP should contain the maximal signal. Its signal strength along the PP would be reduced by, presumably, the same factor of a based on the definition of the $\Delta\gamma$ variable. In other words, in the same event, the CME signal is projected from SP to PP, and the background is projected from PP to SP. With simple algebra, the CME signal fraction in $\Delta\gamma$ can be extracted as [30]

$$f_{\rm CME} = \frac{\Delta\gamma_{\rm CME}\{\rm PP\}}{\Delta\gamma\{\rm PP\}} = \frac{A/a - 1}{1/a^2 - 1}, \tag{3}$$

where

$$A = \Delta\gamma\{\rm SP\}/\Delta\gamma\{\rm PP\}, \tag{4}$$

and the geometry fluctuation factor a can be measured by

$$a = v_2\{\rm SP\}/v_2\{\rm PP\}. \tag{5}$$

The $f_{\rm CME}$ is effectively determined by the quantity A/a, which is the double ratio of $\Delta\gamma/v_2$ w.r.t. SP to that w.r.t. PP.

In reality, due to possible complications of CME signal generation and/or evolution with the bulk medium, the CME signal reduction from SP to PP may not be equal to the same factor a [35]. Suppose the reduction factor is b, i.e., $\Delta\gamma_{\rm CME}\{\rm PP\} = b\Delta\gamma_{\rm CME}\{\rm SP\}$; then it is straightforward to arrive at $f_{\rm CME} = \frac{A/a-1}{1/ab-1}$ following the algebra in Ref. [30]. The difference would be simply a scaling factor $\frac{1/a^2-1}{1/ab-1}$ once b can be reliably obtained from theory. We will not dwell on this complication in our present work, and will simply assume $b = a$ in the paper.

It is important to note that a key assumption in the SP/PP method is that the CME background is proportional to v_2 [30]. This is a good assumption because the CME background of particle correlations, which is intrinsically of nonflow nature, is conveyed by flow to experimental observables [see Eq. (2)]. This assumption, however, breaks down when experimentally measured v_2 itself is also contaminated by nonflow [36]. As a result, the CME fraction extracted by the SP/PP method would be inaccurate, with an inaccuracy depending on the amount of nonflow contamination in v_2. In addition, the proportionality assumption also breaks down when there is contamination from three-particle (3p) nonflow correlations in CME observables, which is often measured by three-point correlators (see below) [10,11]. There is no *a priori* reason to expect such 3p correlations to be proportional to v_2.

Experimentally, the SP can be assessed by the first-order event plane of spectator neutrons measured in zero-degree calorimeters (ZDCs), and the PP can be assessed by the second-order event plane (EP) reconstructed from final-state hadrons [31,32]. For simplicity, we will continue to use SP for the former, but will use EP for the latter to distinguish it from PP as *nonflow* implications are different. Their azimuthal angles are $\Psi_{\rm SP}$ and $\Psi_{\rm EP}$, respectively, and their measurement inaccuracy are corrected by event-plane resolutions [37].

We will use an asterisk on a variable to signal it contains nonflow, and reserve the original one to contain only "true" flow. To calculate the v_2^* and $\Delta\gamma^*$ w.r.t. the EP, the POI should be excluded from the EP reconstruction to avoid self-correlations. Alternatively one may use the cumulant method [37],

$$v_2^* = v_{2,c}^* = \sqrt{\langle \cos 2(\phi_\alpha - \phi_c)\rangle}, \tag{6}$$

where the α and c particles are from the same phase space or from two subevents symmetric about midrapidity having a given pseudorapidity (η) gap; and

$$\begin{aligned} C_3^* &= \langle \cos(\phi_\alpha + \phi_\beta - 2\phi_c)\rangle, \\ \Delta\gamma^* &= C_3^*/v_{2,c}^*, \end{aligned} \tag{7}$$

where the third particle c serves as the EP and its elliptic flow parameter $v_{2,c}^*$ is the EP resolution. (By convention greek subscripts α, β are used to stand for POI, and roman letter c is used for the EP measurement tool.) Again, in Eq. (7), the 3p correlator C_3^* refers to the OS − SS difference. One way to eliminate self-correlations is to separate the POI and the EP, or equivalently the POI and c, in phase space by applying the subevent method. For clarity, we will label these quantities by "{EP}" in this paper, even though they may be calculated by multiparticle cumulants.

Accordingly, the quantities a, A, and $f_{\rm CME}$ in Eqs. (3), (4), and (5) will also be tagged by an asterisk because they are, in turn, all affected by nonflow. In fact, a nonzero $f_{\rm CME}^*$ extracted by the SP/PP method, in the absence of real CME signal, is by definition all coming from nonflow. This is the subject of the present paper.

III. NONFLOW EFFECTS

Flow is a global correlation: all particles in an event are correlated because of their correlations to a common symmetry plane (RP, SP, or PP) [38]. Nonflow, on the other hand, refers to any correlations that do not originate from the global, event-wise azimuthal correlations to a common symmetry plane [39,40]. Those nonflow correlations arise mainly from

two-particle and multiparticle correlations due to resonance decays and jets, or generally cluster correlations [36,40–42]. Other sources of nonflow correlations are of less importance, including Hanbury Brown–Twiss (HBT) correlations from quantum interferometry and correlations due to final-state (post freezeout) interactions such as Coulomb interactions [43].

Because the ZDC measures spectator neutrons, the $v_2\{\mathrm{SP}\}$ of midrapidity particles measured w.r.t. Ψ_{SP} is a good estimate of the "true" elliptic flow (w.r.t. SP); there is little nonflow contamination because spectator neutrons are not dynamic and because of the large η gap between midrapidity and the ZDC.

The PP, on the other hand, is assessed by the EP reconstructed from final-state hadrons. There exist nonflow effects in the reconstructed Ψ_{EP}. The $v_2^*\{\mathrm{EP}\}$ measured w.r.t. Ψ_{EP}, or similarly by the 2p cumulant of Eq. (6), is therefore contaminated by nonflow effect. The nonflow in v_2^* is mainly from 2p correlations (3p ones are comparatively negligible):

$$v_{2,\mathrm{nf}}^2 = \langle \cos 2(\phi_\alpha - \phi_c)\rangle_{\mathrm{nf}} = \frac{C_{\Delta\phi} N_{\Delta\phi}}{2N^2}, \tag{8}$$

where $N_{\Delta\phi}$ is the number of correlated pairs and $C_{\Delta\phi} \equiv \langle \cos 2\Delta\phi\rangle$ is the 2p correlation within the pair. Note $N_{\Delta\phi}$ includes all (*charge-independent*) correlated pairs, not just OS pairs (such as those from resonance decays) but also SS pairs (from jets, etc.). Since $N_{\Delta\phi} \propto N$, nonflow decreases with increasing multiplicity. In general, the $v_2^*\{\mathrm{EP}\}$ from 2p cumulant contains both flow and nonflow:

$$v_2^*\{\mathrm{EP}\} = \sqrt{v_2^2\{\mathrm{EP}\} + v_{2,\mathrm{nf}}^2}. \tag{9}$$

The major background contribution to $\Delta\gamma$ is the flow-induced background, given by Eq. (2). Let us refer to this contribution as $C_{3,2\mathrm{p}}$, standing for 2p contribution to the 3p correlator C_3. In terms of C_3, before $v_{2,c}^* = v_2^*$ is divided out, we have

$$C_{3,2\mathrm{p}} = \frac{C_{2\mathrm{p}} N_{2\mathrm{p}}}{N^2} v_{2,2\mathrm{p}} v_2. \tag{10}$$

Note that the correlation between the 2p pair and particle c here is due to pure flow (nonflow effect is discussed below), so what matter in Eq. (10) are their true flows ($v_{2,2\mathrm{p}}$ and v_2, without asterisk marks). Although one element of this background is 2p nonflow correlations as previously discussed, we do not label the left-hand side quantity by an asterisk but consider it as flow induced. We have taken the shorthand notation for the charge-dependent 2p correlation as $C_{2\mathrm{p}} = \langle \cos(\phi_\alpha + \phi_\beta - 2\phi_{2\mathrm{p}})\rangle$.

Note the form of Eq. (10) is the same for both EP and SP, so we simply use $v_{2,2\mathrm{p}}$ and v_2 to refer to those w.r.t. SP or EP. This background is the main background in the 3p correlator, and is present in both $C_3\{\mathrm{EP}\}$ and $C_3\{\mathrm{SP}\}$, proportional to the respective $v_2\{\mathrm{EP}\}$ and $v_2\{\mathrm{SP}\}$. This proportionality, together with the inverse proportionality of the CME effect, renders the validity of the SP/PP method as discussed previously.

There is an additional background contribution to $\Delta\gamma^*\{\mathrm{EP}\}$; this is the charge-dependent (i.e., between the α and β POIs but irrespective of the charge of particle c) 3p nonflow correlations to C_3^*, and subsequently propagated to $\Delta\gamma^* = C_3^*/v_2^*$. It can be expressed as

$$C_{3,3\mathrm{p}}^*\{\mathrm{EP}\} = \frac{C_{3\mathrm{p}} N_{3\mathrm{p}}}{2N^3}, \tag{11}$$

where $N_{3\mathrm{p}}$ is the number of correlated 3p triplets, and $C_{3\mathrm{p}} = \langle \cos(\phi_\alpha + \phi_\beta - 2\phi_c)\rangle_{3\mathrm{p}}$ where the three particles (α, β, c) belong to the same triplet. A major source of the charge-dependent 3p nonflow correlations may come from dijet correlations. The total 3p correlators are therefore given by

$$C_3\{\mathrm{SP}\} = \frac{C_{2\mathrm{p}} N_{2\mathrm{p}}}{N^2} v_{2,2\mathrm{p}}\{\mathrm{SP}\} v_2\{\mathrm{SP}\}, \tag{12a}$$

$$C_3^*\{\mathrm{EP}\} = \frac{C_{2\mathrm{p}} N_{2\mathrm{p}}}{N^2} v_{2,2\mathrm{p}}\{\mathrm{EP}\} v_2\{\mathrm{EP}\} + \frac{C_{3\mathrm{p}} N_{3\mathrm{p}}}{2N^3}. \tag{12b}$$

Note again that we have taken the "C" quantities to refer to the OS − SS differences (i.e., charge dependent, where the charge refers to the α, β particles).

IV. SIMULATION RESULTS

In this section, we use the AMPT model [44,45] and the HIJING model [46,47] to simulate Au+Au collisions at $\sqrt{s_{NN}} =$ 200 GeV. No CME signal is included in either model. The AMPT version is v1.25t4cu2/v2.25t4cu2, in which string melting is implemented. In AMPT simulation hadronic cascade is included by setting the parameter `NTMAX = 150`. Unlike in earlier versions, in this version local charge conservation is ensured [48]; global charge conservation is automatically satisfied. The HIJING version is v1.411. In HIJING simulation jet quenching is turned on.

These models contain the essential physics of nonflow correlations, although neither of them may be complete. HIJING gives a fair description of hard scattering and jet fragmentation [46], as well as jet quenching in heavy ion collisions [49]. It can therefore yield reasonable estimate of jet contributions to nonflow correlations [50–52]. HIJING models soft particle production through the phenomenology of string excitation and fragmentation [53–55], and hence has a reasonable parametrization of resonance decay contributions to nonflow [56,57]. The AMPT model is initialized by the hadrons produced by HIJING [44]. In its string melting version [58] that we use in our simulation, those hadrons are dissolved into quarks which scatter with other quarks in the subsequent parton transport evolution. The correlations among hadrons from dominantly low-p_T jets (minijets) are largely destroyed. As a result, AMPT does not have adequate nonflow contribution from jets [59]. The purpose of the string-melting version of AMPT is to describe anisotropic flow and particle production data [58]. Indeed, AMPT gives a reasonable description of particle and resonance yields and transverse momentum distributions [60], therefore the bulk of resonance decay nonflow contributions. AMPT can also reasonably describe the measured correlations [61]. Because the charge is conserved process by process [48] in the used version of AMPT, local charge conservation and cluster correlations as part of its parton transport are preserved. Although AMPT may not include enough jet correlation contributions, studies indicate that it may contain too much nonflow [62], overestimating data as we also find, as discussed in Sec. V. In our estimates, we

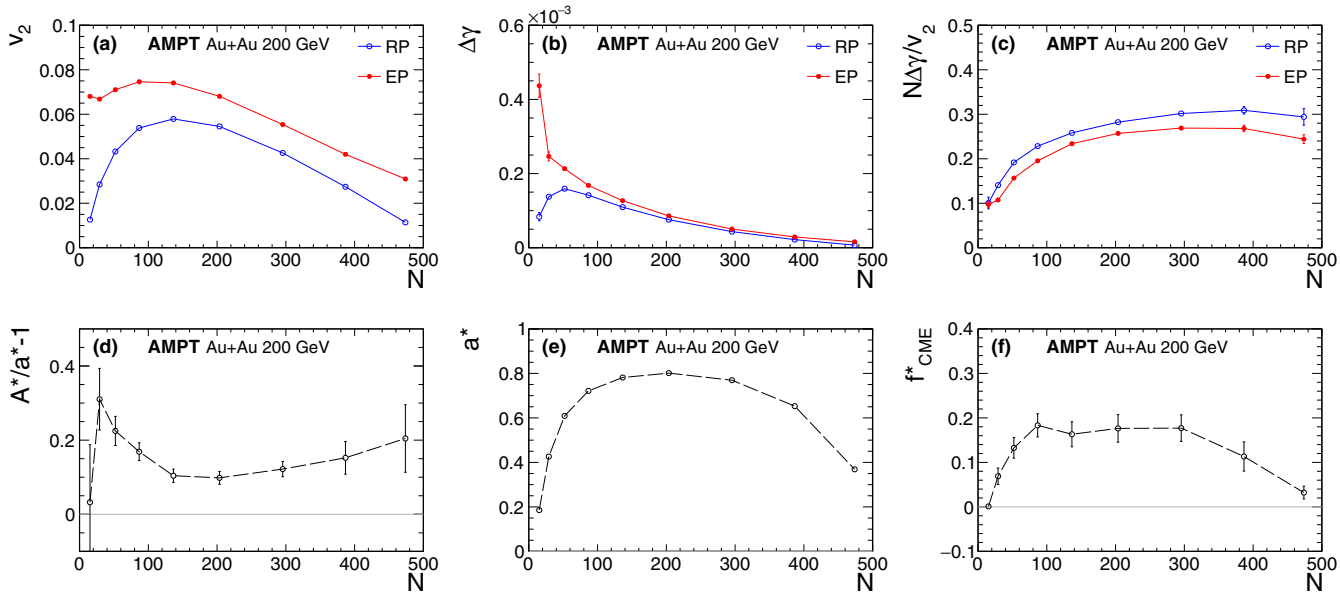

FIG. 1. AMPT simulation results as functions of $N = (N_+ + N_-)/2$, the POI single-charge multiplicity, in 200 GeV Au+Au collisions: (a) elliptic flow v_2, (b) charge-dependent 3p correlator $\Delta\gamma$, (c) $N\Delta\gamma/v_2$ w.r.t. RP and EP [the former is referred to as $\epsilon_2^{\rm AMPT}$; see Eqs. (2) and (13)], (d) $A^*/a^* - 1$ [$\equiv \epsilon_{\rm AMPT}$, which approximately equals the nonflow contamination $\epsilon_{\rm nf}$ in v_2; see Eqs. (15) and (17)], (e) a^* by Eq. (18), and (f) the calculated $f^*_{\rm CME}$ by Eq. (3). The POI and particle c (for EP) are from $|\eta| < 1$ and $0.2 < p_T < 2$ GeV/c. All errors are statistical, with total 3.77×10^8 AMPT minibias events.

attempt to use data, wherever available, to constrain the model estimates of nonflow contributions.

In our simulations, about 3.77×10^8 and 5.92×10^8 minibias events (impact parameter range $0 < b < 16$ fm) are generated by AMPT and HIJING, respectively. We divide those events into nine centrality bins corresponding to 0–5%, 5–10%, 10–20%, 20–30%, 30–40%, 40–50%, 50–60%, 60–70%, and 70–80% of all events generated, according to the midrapidity charged hadron multiplicity within $|\eta| < 0.5$, similar to what is done in the STAR experiment [63,64]. We will display our results as functions of centrality percentile and $dN/d\eta$, the corresponding charged hadron multiplicity pseudorapidity density, which is approximately the single-charge POI multiplicity (N) within $|\eta| < 1$.

For RP, we simply used $\Psi_{\rm RP} = 0$ as set in the models. It is also a good estimation of the SP, so we will use RP in place of SP. The PP can be estimated by the EP reconstructed from particles in the same phase space as the POI, defined to be hadrons within $|\eta| < 1$ and $0.2 < p_T < 2.0$ GeV/c (or $0.2 < p_T < 1.0$ GeV/c) in this study. As mentioned, the EP method can be replaced by particle cumulant method in calculating v_2^* (and also C_3^*) as we adopted in this work. They contain nonflow contributions because of particle correlations.

Figure 1(a) shows the $v_2\{\rm RP\}$ and $v_2^*\{\rm EP\}$ as functions of N in AMPT. The $v_2^*\{\rm EP\}$ is significantly larger than the $v_2\{\rm RP\}$, primarily because of geometry fluctuations (so $v_2\{\rm EP\} > v_2\{\rm RP\}$); this difference is exploited in the SP/PP method. In addition, there is a relatively minor contribution from nonflow to the difference (i.e., $v_2^*\{\rm EP\} > v_2\{\rm EP\}$); although minor in the difference, it has non-negligible effect on the extracted $f^*_{\rm CME}$ as we discuss in this paper. Figure 1(b) shows the $\Delta\gamma\{\rm RP\}$ calculated w.r.t. RP and $\Delta\gamma^*\{\rm EP\}$ calculated by the 3p correlator in AMPT. The $\Delta\gamma^*\{\rm EP\}$ is larger than the $\Delta\gamma\{\rm RP\}$, primarily because of the correspondingly larger $v_2\{\rm EP\}$ than $v_2\{\rm RP\}$ [see Eq. (10)]. Since AMPT "destroys" minijets from HIJING in its model initialization, the $C_3^*\{\rm EP\}$ may have little 3p nonflow contributions, so we may assume $C_3^*\{\rm EP\} \approx C_3\{\rm EP\}$. Under this assumption, according to Eqs. (10) and (7), the $\Delta\gamma\{\rm EP\}/v_2\{\rm EP\}$ and $\Delta\gamma\{\rm RP\}/v_2\{\rm RP\}$ would be the same after properly accounting for the respective true flow v_2, because presumably $v_{2,2\rm p}\{\rm EP\}/v_2\{\rm EP\} = v_{2,2\rm p}\{\rm RP\}/v_2\{\rm RP\}$. Thus we show in Fig. 1(c) the ratios of $N\Delta\gamma\{\rm RP\}/v_2\{\rm RP\}$ and $N\Delta\gamma^*\{\rm EP\}/v_2^*\{\rm EP\}$, where N is multiplied to better show the magnitudes. The former is the following charge-dependent 2p correlation strength [see Eqs. (10) and (7)]:

$$\epsilon_2 \equiv \frac{C_{2\rm p} N_{2\rm p} v_{2,2\rm p}}{N v_2}; \tag{13}$$

namely,

$$\epsilon_2 = N\frac{\Delta\gamma\{\rm RP\}}{v_2\{\rm RP\}} = N\frac{\Delta\gamma\{\rm EP\}}{v_2\{\rm EP\}}. \tag{14}$$

We will refer to this ϵ_2 from AMPT as $\epsilon_2^{\rm AMPT}$. It increases somewhat from peripheral to central collisions. The value $\epsilon_2^{\rm AMPT} \approx 0.3$–$0.4$ in mid-central to central collisions makes sense as we roughly expect $C_{2\rm p} \approx 0.65$, $N_{2\rm p}/N \approx 0.3$, $v_{2,2\rm p}/v_2 \approx 2$ [23].

The $v_2\{\rm EP\}$ without nonflow contamination is of course unknown *a priori*; one measures only the nonflow contaminated $v_2^*\{\rm EP\}$. That is,

$$\frac{\Delta\gamma^*\{\rm EP\}}{v_2^*\{\rm EP\}} = \frac{C_3\{\rm EP\}}{v_2^*\{\rm EP\}^2} = \frac{\epsilon_2}{N}\frac{1}{1+\epsilon_{\rm nf}}, \tag{15}$$

where

$$\epsilon_{\rm nf} \equiv v_{2,\rm nf}^2/v_2^2, \tag{16}$$

and we have assumed no charge-dependent 3p nonflow contributions in AMPT (i.e., $C_3^*\{\rm EP\} \approx C_3\{\rm EP\}$) as aforementioned. Because of the nonflow in $v_2^*\{\rm EP\}$, the $\Delta\gamma^*\{\rm EP\}/v_2^*\{\rm EP\}$ is slightly smaller than the $\Delta\gamma\{\rm RP\}/v_2\{\rm RP\}$. In turn, the quantity

$$\frac{A^*}{a^*} = \frac{\Delta\gamma\{\rm RP\}/v_2\{\rm RP\}}{\Delta\gamma^*\{\rm EP\}/v_2^*\{\rm EP\}} \tag{17}$$

is larger than unity; let us denote $\epsilon_{\rm AMPT} \equiv A^*/a^* - 1$, shown in Fig. 1(d). If there are no charge-dependent 3p correlations in AMPT, then $\epsilon_{\rm AMPT} = \epsilon_{\rm nf}$ [see Eq. (15)] would be a good estimate of the nonflow in v_2^* from AMPT; Fig. 1(d) indicates that it is on the order of 10–20% depending on centrality. This recipe of estimating nonflow by $A^*/a^* - 1$ cannot be readily applied to real data because of the potential 3p nonflow contributions to $\Delta\gamma^*\{\rm EP\}$ in the real data, which we will discuss later. Of course, if AMPT also contains significant charge-dependent 3p nonflow correlations, then the $\epsilon_{\rm nf}$ estimate here is also questionable. We will return to this point in Sect. V.

From Eq. (3), the larger-than-unity A^*/a^* would result in a positive $f_{\rm CME}^* = \epsilon_{\rm AMPT}/(1/a^{*2} - 1)$. Here the factor a^* is measured by

$$a^* = v_2\{\rm RP\}/v_2^*\{\rm EP\} = a/\sqrt{1+\epsilon_{\rm nf}}, \tag{18}$$

which is shown in Fig. 1(e). The $f_{\rm CME}^*$ due to nonflow basically equals $\epsilon_{\rm nf} \approx \epsilon_{\rm AMPT}$ multiplied by a factor determined by a^* (or a as the nonflow effect in a^* makes a minor correction). With the $\epsilon_{\rm nf}$ of the order of 10% and $a \approx 0.8$ in mid-central collisions, an $f_{\rm CME}^*$ value of the order of 20% can result, as shown in Fig. 1(f). This is a significant effect, whereas AMPT itself of course does not contain any CME. It is worthwhile to note, however, that the $\epsilon_{\rm nf}$ in AMPT shown in Fig. 1(d) may not be an accurate estimate of nonflow in experimental data, and AMPT does not have significant 3p correlations that may be present in real data. Both of these affect the estimate of nonflow contributions to $f_{\rm CME}^*$; we will return to this in Sec. V.

Let us now turn to HIJING. Figure 2(a) shows the $v_2\{\rm RP\}$ and $v_2^*\{\rm EP\}$ from HIJING as functions of N. The small but negative $v_2\{\rm RP\}$ is a result of jet quenching: more particles are generated perpendicular to the RP because of the longer path lengths jets traverse. Such an azimuthal modulation is global and technically has no distinction from "real" flow, so we will just refer to it in this paper as "true" v_2. Figure 2(a) shows that the $v_2^*\{\rm EP\}$ is significantly larger and positive. The major contribution to $v_2^*\{\rm EP\}$ in HIJING is nonflow; the jet-quenching induced anisotropy is negligible in $v_2^*\{\rm EP\}$. Thus, the flow-induced background $\Delta\gamma_{\rm bkgd}$ of Eq. (2) or (10) is small in HIJING; the $\Delta\gamma^*\{\rm EP\}$ in Eq. (12b) will be dominated by the second term, 3p nonflow correlations. In a previous work [59], we have shown that $N\Delta\gamma^*\{\rm EP\}/v_2^*\{\rm EP\}$ in HIJING is large and has a weak centrality dependence, indicating a good degree of factorization of the 3p (such as dijet) correlations into 2p correlations. In Fig. 2(b) we show directly the 3p correlators, multiplied by N^2, namely $N^2C_3^*\{\rm EP\}$ and $N^2C_3\{\rm RP\}$. It is shown, indeed, that $C_3^*\{\rm EP\}$ is significantly larger than

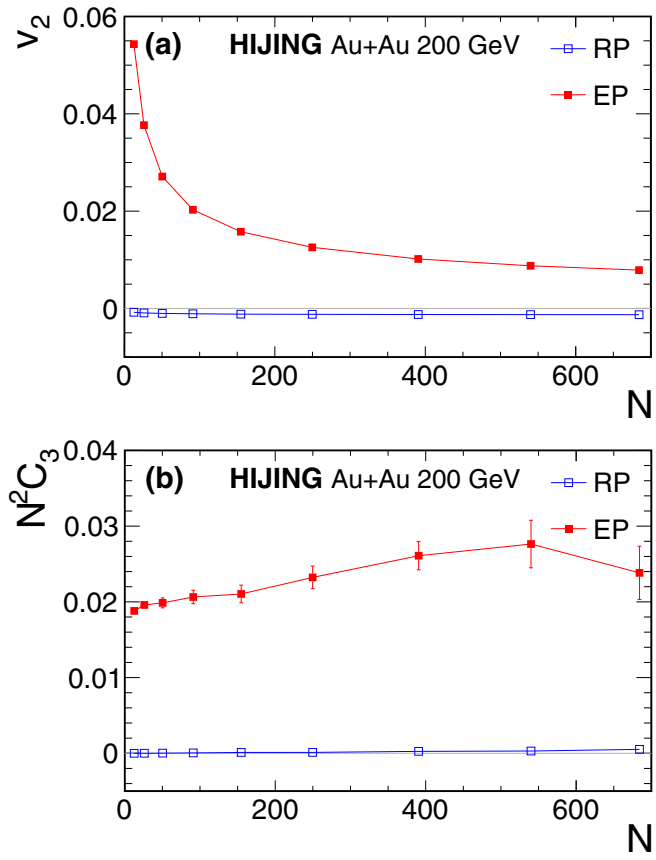

FIG. 2. HIJING simulation results as functions of $N = (N_+ + N_-)/2$, the POI single-charge multiplicity, in 200 GeV Au+Au collisions: (a) elliptic anisotropy v_2, and (b) charge-dependent 3p correlator N^2C_3 w.r.t. RP and EP [the latter is referred to as $\epsilon_3 = \epsilon_3^{\rm HIJING}$; see Eqs.(11), (12b), and (19)]. The POI and particle c are from $|\eta| < 1$ and $0.2 < p_T < 2$ GeV/c. All errors are statistical, with 5.92×10^8 HIJING minibias events.

$C_3\{\rm RP\}$, with the latter being negligible. This indicates that the 3p nonflow contribution dominates in $C_3^*\{\rm EP\}$ over the "flow"-induced contribution in HIJING. The $N^2C_3^*\{\rm EP\}$ in Fig. 2(b), which we will refer to as $\epsilon_3^{\rm HIJING}$, essentially gives the charge-dependent 3p correlation strength [see Eq. (11)],

$$\epsilon_3 \equiv \frac{C_{3\rm p}N_{3\rm p}}{2N}. \tag{19}$$

Its strength has only modest increase with centrality in HIJING.

Unlike AMPT, HIJING does not have a significant flow-induced background, so it is not meaningful to extract a $f_{\rm CME}^*$ value from HIJING like we did for AMPT. However, the 3p nonflow correlations in HIJING, that AMPT lacks, are useful knowledge to assess additional nonflow effect in a real data analysis, which we now attend to.

V. IMPLICATIONS TO REAL DATA

Real experimental data are probably similar to AMPT in terms of flow, and likely contain 3p correlations similar to

HIJING. According to Eq. (12b) we can write

$$\frac{\Delta\gamma^*\{\mathrm{EP}\}}{v_2^*\{\mathrm{EP}\}} = \frac{\epsilon_2}{N}\cdot\frac{1+\frac{\epsilon_3/\epsilon_2}{Nv_2^2\{\mathrm{EP}\}}}{1+\epsilon_{\mathrm{nf}}}, \tag{20}$$

where $\frac{\epsilon_3/\epsilon_2}{Nv_2^2\{\mathrm{EP}\}} = \frac{C^*_{3,3p}}{C_{3,2p}}$ [see Eqs. (10) and (11)] is just the relative 3p over 2p contributions to the 3p correlator. Measurements w.r.t. RP are not affected by nonflow, so we simply have $\Delta\gamma\{\mathrm{RP}\}/v_2\{\mathrm{RP}\} = \epsilon_2/N$. From Eq. (3), we obtain

$$f^*_{\mathrm{CME}} = \left(\frac{1+\epsilon_{\mathrm{nf}}}{1+\frac{\epsilon_3/\epsilon_2}{Nv_2^2\{\mathrm{EP}\}}}-1\right)\Bigg/\left(\frac{1+\epsilon_{\mathrm{nf}}}{a^2}-1\right) \tag{21a}$$

$$= \left(\frac{1+\epsilon_{\mathrm{nf}}}{1+\frac{(1+\epsilon_{\mathrm{nf}})\epsilon_3/\epsilon_2}{Nv_2^{*2}\{\mathrm{EP}\}}}-1\right)\Bigg/\left(\frac{1}{a^{*2}}-1\right). \tag{21b}$$

The 2p nonflow effect, ϵ_{nf}, increases 2p cumulant $v_2^*\{\mathrm{EP}\}$, and consequently introduces a positive f^*_{CME} (as in AMPT). The 3p nonflow effect, ϵ_3, increases $C_3^*\{\mathrm{EP}\}$ and $\Delta\gamma^*\{\mathrm{EP}\}$, and consequently introduces a negative f^*_{CME}. That the two nonflow effects cancel each other to some degree is a neat feature, making the f^*_{CME} from the RP/PP method less vulnerable to nonflow. The quantitative conclusion depends of course on the relative magnitudes of the nonflow effects from 2p and 3p correlations.

It is worthwhile to note that, because $\epsilon_3 \ll \epsilon_2$ [by comparing Fig. 1(c) and Fig. 2(b)] and normally $Nv_2^2 \sim O(1)$, the flow-induced background (due to charge-dependent 2p correlations) is the leading order term in C_3^* (and $\Delta\gamma^*\{\mathrm{EP}\}$) and the charge-dependent 3p nonflow correlations are the next-to-leading order (NLO) perturbation; meanwhile the NLO perturbation in v_2^* is the nonflow from charge-independent 2p correlations and the charge-independent 3p nonflow correlations can be neglected. To the order of the respective NLO terms of v_2^* and C_3^*, we may write

$$f^*_{\mathrm{CME}} \approx \left(\epsilon_{\mathrm{nf}} - \frac{\epsilon_3/\epsilon_2}{Nv_2^2\{\mathrm{EP}\}}\right)\Bigg/\left(\frac{1+\epsilon_{\mathrm{nf}}}{a^2}-1\right) \tag{22a}$$

$$= \left(\epsilon_{\mathrm{nf}} - \frac{(1+\epsilon_{\mathrm{nf}})\epsilon_3/\epsilon_2}{Nv_2^{*2}\{\mathrm{EP}\}}\right)\Bigg/\left(\frac{1}{a^{*2}}-1\right). \tag{22b}$$

However, since nonflow ϵ_{nf} and $(\epsilon_3/\epsilon_2)/(Nv_2^2)$ may not always be small compared to unity (e.g., in peripheral collisions), we will nonetheless use Eq. (21) to estimate the magnitudes of the nonflow effects in f^*_{CME}.

The estimate of the 2p nonflow effect boils down to the estimate of ϵ_{nf}. If ϵ_{nf} is as given by AMPT [i.e., $\epsilon_{\mathrm{nf}} = \epsilon_{\mathrm{AMPT}}$ as in Fig. 1(d)], then its effect on f^*_{CME} would be that shown in Fig. 1(f). Nonflow has been extensively studied in real data. A data-driven way to estimate nonflow contribution is performed by STAR [65]. We show in Fig. 3 the estimated nonflow $\epsilon_{\mathrm{nf}}^{\mathrm{exp}}$ in Au+Au collisions for $|\Delta\eta| > 0.7$ scaled up by a factor of 2.0 to represent the nonflow contributions without any η gap [65]. The systematic uncertainties on the data vary between 20% and 50%. Also shown in Fig. 3 by the open circles are the ϵ_{AMPT} from AMPT [i.e., the data points in Fig. 1(d)]. These would be the nonflow ϵ_{nf} in AMPT if charge-dependent 3p correlations to $\Delta\gamma^*\{\mathrm{EP}\}$ can be neglected. (The filled circles represent

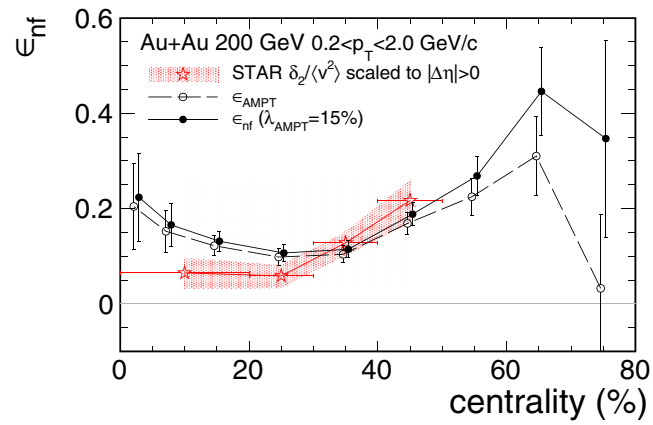

FIG. 3. Estimated v_2 nonflow as functions of centrality in 200 GeV Au+Au collisions (data points are slightly shifted in the horizontal axis for clarity). The open (filled) circles are from AMPT, assuming 0% (15%) charge-dependent 3p contributions to $\Delta\gamma^*\{\mathrm{EP}\}$. Errors are statistical. The red stars are STAR data [65], where the systematic uncertainties are ±50% for centrality 0–20%, ±40% for 20–30%, and ±20% for 30–50%.

those with 3p correlations considered, as explained later in the text.) The nonflow contribution depends on centrality. In 20–30% or more central collisions, AMPT somewhat overestimates the data. In more peripheral collisions, AMPT seems to underestimate the data. Measurements are unavailable for the peripheral 50–80% centralities. We extrapolate to those peripheral centralities by fitting the ratio of data over AMPT with a linear dependence: $\epsilon_{\mathrm{nf}}^{\mathrm{exp}}/\epsilon_{\mathrm{AMPT}} = 2.08 \times \mathrm{cent} + 0.25$, where the centrality "cent" is a number between 0 and 1. We scale the AMPT nonflow ϵ_{AMPT} (assuming zero 3p contribution) shown by the open circles in Fig. 3 by the fitted linear function. We use the scaled ϵ_{nf} value to evaluate its contribution to f^*_{CME} by the first term of Eq. (22b), $\epsilon_{\mathrm{nf}}/(\frac{1}{a^{*2}}-1)$, where a^* is taken from Fig. 1(e). The result is shown in Fig. 4 as function of centrality by the open circles where the statistical errors are from the AMPT simulation data sample and the open band embraces the experimental uncertainty on nonflow of ±20–50% (for the extrapolated peripheral range, we assume the same systematic uncertainty of ±20% as that in the 20–30% centrality bin).

It is worthwhile to note that here we have effectively used experimental nonflow results in the estimate of f^*_{CME}, by scaling ϵ_{AMPT} to $\epsilon_{\mathrm{nf}}^{\mathrm{exp}}$. Using AMPT as a stepping stone seems unnecessary except for the extrapolation to peripheral collisions. However, we will also investigate nonflow effects in other kinematic regions later in the article where experimental data on nonflow are not readily available. There, we will need to use AMPT simulation results and scale them by assuming the same scaling factor as a function of centrality parametrized here.

The 3p nonflow effect in f^*_{CME} can be estimated as follows. The ϵ_3 can be obtained from HIJING in Fig. 2(b), $\epsilon_3^{\mathrm{HIJING}} = N^2C_3^*\{\mathrm{EP}\}$, because it has been observed to give a fair description of the small-system collision data at RHIC within 20% [59]; so we take $\epsilon_3 = \epsilon_3^{\mathrm{HIJING}} \pm 20\%$. The flow and flow fluctuation related quantities $Nv_2^{*2}\{\mathrm{EP}\}$ and a^* can

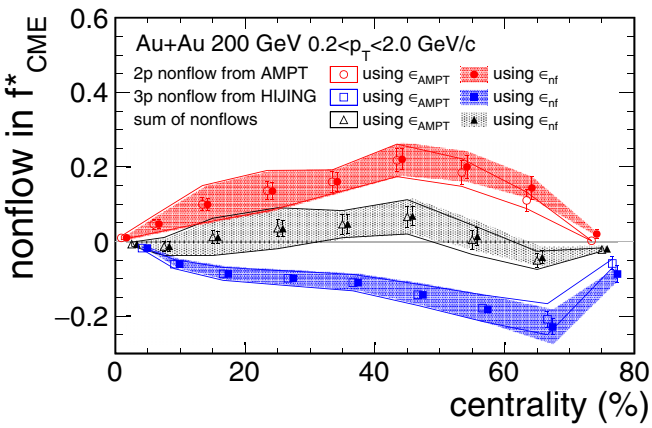

FIG. 4. The 2p and 3p nonflow contributions [by Eq. (22)] and their net contribution [Eq. (21) to $f^*_{\rm CME}$ as functions of centrality in 200 GeV Au+Au collisions, with elliptic flow and geometry fluctuation effect (i.e., a^*) taken from AMPT, and with various assumptions of nonflow contributions. Open markers: charge-independent 2p nonflow as in AMPT, $\epsilon_{\rm nf} = \epsilon_{\rm AMPT}$ as from Fig. 1(d) [i.e., 3p contribution $\lambda_{\rm AMPT} = 0$ in Eq. (23)] and scaled to experimental measurement [65] (open circles), charge-dependent 3p nonflow correlations as in HIJING, $\epsilon_3 = \epsilon_3^{\rm HIJING} \pm 20\%$ (open squares), and the sum of the two (open triangles); the open bands are the respective systematic uncertainties in matching to experimental data. Solid markers are corresponding nonflow effects, as open markers but with $\lambda_{\rm AMPT} = 15\%$ in Eq. (23), the charge-dependent 3p correlations in AMPT relative to those in HIJING; the shaded bands are the corresponding systematic uncertainties. The POI and particle c are from $|\eta| < 1$ and $0.2 < p_T < 2$ GeV/c. Data points are slightly shifted in the horizontal axis for clarity.

be taken from AMPT. The ϵ_2 can also be taken from AMPT in Fig. 1(c), but it has been observed that AMPT can reproduce only about 60% of the $\Delta\gamma^*/v_2^*$ in real data [59]; so we take $\epsilon_2 = 1.7\epsilon_2^{\rm AMPT}$. (Note that this underestimate of ϵ_2 by AMPT does not directly affect the first term of Eq. (21), because it appears in both $\Delta\gamma^*\{\rm EP\}$ and $\Delta\gamma\{\rm RP\}$ and is canceled. The ϵ_2 (charge-dependent 2p nonflow) does contribute, in part, to the $\epsilon_{\rm nf}$ (charge-independent 2p nonflow), but there are many other charge-independent contributions (e.g., like-sign particle correlations) that apparently have resulted in an already overestimated $\epsilon_{\rm nf} \approx 10$–$20\%$ in AMPT for mid-central collisions, as mentioned.) The estimated 3p nonflow effect by the second term of Eq. (22b), $-\frac{(1+\epsilon_{\rm nf})\epsilon_3/\epsilon_2}{Nv_2^{*2}\{\rm EP\}}/(\frac{1}{a^{*2}}-1)$, is shown in Fig. 4 in the open squares with small statistical error bars from the large HIJING simulation data sample. The open band indicates the $\pm 20\%$ systematic uncertainty, the level of agreement of HIJING in describing experimental data.

The combination of the two, as given by Eq. (21), would indicate the error one makes in $f^*_{\rm CME}$ extracted from "experimental" data, if the 2p and 3p nonflow effects are as given by AMPT ($\epsilon_{\rm nf} = \epsilon_{\rm AMPT}$, scaled to $\epsilon_{\rm nf}^{\rm exp}$) and HIJING ($\epsilon_3 = \epsilon_3^{\rm HIJING} \pm 20\%$), respectively. This is shown as the open triangles in Fig. 4. The accompanying open band is the quadratic sum of the systematic uncertainty estimates on $\epsilon_{\rm nf}$ and ϵ_3. Note that the net result is not a simple sum of the individual 2p and 3p nonflow effects estimated above via the approximated Eq. (22b), which is only valid when both effects are small. As shown by Fig. 4, nonflow correlations could contribute an artificial $f^*_{\rm CME}$ signal up to a few percent (in both positive and negative directions), depending on centrality, in Au+Au collisions at 200 GeV.

In estimating nonflow effects in $f^*_{\rm CME}$ by Eqs. (21) and (22), we have used AMPT to estimate the nonflow effect $\epsilon_{\rm nf}$ in v_2 and HIJING to estimate the 3p nonflow effect ϵ_3 in $\Delta\gamma^*\{\rm EP\}$. We have so far neglected 3p correlations in AMPT and attributed the $\Delta\gamma^*$ (and $f^*_{\rm CME}$) in AMPT all to 2p nonflow, so that $\epsilon_{\rm nf} = \epsilon_{\rm AMPT}$. However, AMPT does contain some 3p correlations, approximately $\lambda_{\rm AMPT} = 15\%$ of those from HIJING as shown by the small-system simulations in Ref. [59], presumably due to an incomplete destruction of minijet correlations in AMPT model initialization. Since these 3p correlations contribute a negative magnitude to $f^*_{\rm CME}$, the 2p nonflow effect $\epsilon_{\rm nf}$ would be larger than the $\epsilon_{\rm AMPT}$ depicted in Fig. 1(f). In other words, following Eq. (21),

$$\epsilon_{\rm nf} = \epsilon_{\rm AMPT} + \lambda_{\rm AMPT}\frac{(1+\epsilon_{\rm nf})\epsilon_3/\epsilon_2}{Nv_2^{*2}\{\rm EP\}}, \tag{23}$$

from which we can deduce a new $\epsilon_{\rm nf}$ in AMPT. This is shown by the filled circles in Fig. 3. (Note that the $\lambda_{\rm AMPT} = 15\%$ residual 3p correlation in AMPT is only used to calculate an improved $\epsilon_{\rm nf}$ by Eq. (23); it is not used for any estimate of the 3p correlation contribution to $\Delta\gamma^*\{\rm EP\}$, which is obtained from HIJING in our study.) We again fit a linear function to the ratio of data over AMPT in Fig. 3, $\epsilon_{\rm nf}^{\rm exp}/\epsilon_{\rm nf}(\lambda_{\rm AMPT} = 15\%) = 1.86 \times {\rm cent} + 0.24$, and then scale the $\epsilon_{\rm nf}(\lambda_{\rm AMPT} = 15\%)$ by the fitted function. The resultant $f^*_{\rm CME}$ by Eqs. (22b) and (22b) are depicted in Fig. 4 as the solid markers and shaded bands; note that $\epsilon_{\rm nf}$ affects numerically both 2p and 3p nonflow terms. As seen from Fig. 4, the end results are not much affected by $\lambda_{\rm AMPT}$; this is because the experimental $\epsilon_{\rm nf}^{\rm exp}$ is effectively used in the estimate. Averaging over 20–50% centrality, the effect is approximately $f^*_{\rm CME} = (4 \pm 5)\%$. This is for the case where both the POI and particle c (or EP) are from $|\eta| < 1$ and $0.2 < p_T < 2$ GeV/c (referred to as the full-event method).

One can reduce nonflow effects by applying an η gap between POI and particle c, or simply using the subevent method where the POI are from one subevent and c from the other. Figure 5 shows the average $f^*_{\rm CME}$ within the 20–50% centrality range from the subevent method with various η gaps, together with that from the full-event method given in Fig. 4. The $\Delta\eta$ values are the η gaps between the two subevents that are symmetric about midrapidity. We have used $\lambda_{\rm AMPT} = 15\%$ and scaled the obtained $\epsilon_{\rm nf}$ from AMPT by the same factor used to match the $\epsilon_{\rm nf}^{\rm exp}$ in the full-event method. Once an η gap is applied, AMPT gives significantly reduced $f^*_{\rm CME}$ values because of the significantly reduced nonflow $\epsilon_{\rm nf}$ contamination (note that the average interparticle η gap is significantly larger than the $\Delta\eta$ value between the subevents). The $f^*_{\rm CME}$ resulting from HIJING 3p nonflow is, however, not much reduced. This is consistent with the fact that the 3p nonflow in HIJING is primarily due to dijet correlations which are not much affected by the η gap. As a result, the subevent method gives an overall negative $f^*_{\rm CME}$, approximately $f^*_{\rm CME} = (-5 \pm 3)\%$.

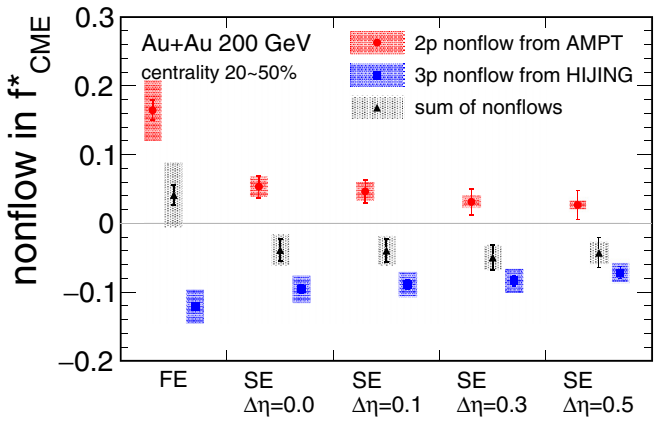

FIG. 5. Same as the solid markers in Fig. 4, but showing the average $f^*_{\rm CME}$ within 20–50% centrality in 200 GeV Au+Au collisions, obtained from the full-event (FE) method (i.e., those in Fig. 4) along with those from the subevent (SE) method with various η gaps. The POI and particle c are from $|\eta| < 1$ and $0.2 < p_T < 2$ GeV/c.

The largest uncertainty of our nonflow estimates comes from those on the experimental nonflow $\epsilon^{\rm exp}_{\rm nf}$ measurements [65]. To give another assessment, we show in Fig. 6 the nonflow estimates taking $\epsilon_{\rm nf} = \epsilon_{\rm AMPT}$ directly from AMPT [as shown in Fig. 1(d)], without the multiplicative factor to match to data $\epsilon^{\rm exp}_{\rm nf}$. Both $\lambda_{\rm AMPT} = 15\%$ and 0% results are shown (their difference is insignificant) where the error bars are statistical as from the models. These are generally within the systematic uncertainties of our estimates in the solid triangles, indicating the robustness of our estimates.

Nonflow has strong p_T dependence; dijet correlations are more significant at high p_T as modeled in HIJING. We repeat our analysis separating the POI (and particle c) into two p_T bins: $0.2 < p_T < 1$ GeV/c and $1 < p_T < 2$ GeV/c (with the same $|\eta| < 1$ range). The results are shown in Fig. 7 by the crosses. The 2p nonflow is taken from AMPT scaled

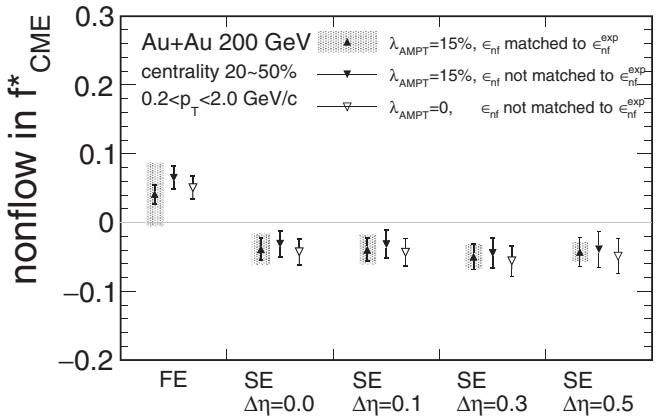

FIG. 6. The nonflow $f^*_{\rm CME}$ in 20–50% Au+Au collisions obtained with various estimates of $\epsilon_{\rm nf}$: from AMPT via Eq. (23) with $\lambda_{\rm AMPT} = 15\%$ and scaled to data $\epsilon^{\rm exp}_{\rm nf}$ [65] (i.e., solid triangles from Fig. 5), and not scaled to data, one with $\lambda_{\rm AMPT} = 15\%$ (inversed solid triangles) and the other $\lambda_{\rm AMPT} = 0\%$ (inversed open triangles). The POI and particle c are from $|\eta| < 1$ and $0.2 < p_T < 2$ GeV/c.

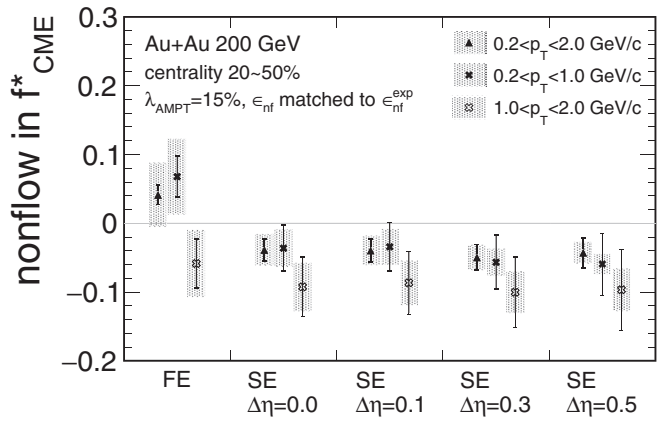

FIG. 7. Same as the solid triangles in Fig. 5, but with two additional sets of data points of split p_T ranges for the POI and particle c: $0.2 < p_T < 1$ GeV/c (filled crosses) and $1 < p_T < 2$ GeV/c (open crosses).

by the centrality-dependent parametrization from the $0.2 < p_T < 2.0$ GeV/c range in Fig. 3. It may be reasonable at low p_T, but is unlikely to be correct at high p_T as AMPT destroys minijet correlations at its initialization. The 3p nonflow which we take from HIJING should be reasonable at high p_T and may likely be so at low p_T as well. Nevertheless, the nonflow effect for $0.2 < p_T < 1$ GeV/c is similar to that for $0.2 < p_T < 2$ GeV/c. We observe a more negative $f^*_{\rm CME}$ for $1 < p_T < 2$ GeV/c although the statistical uncertainties are significantly larger (note the full p_T range contains more statistics than the sum of the two individual p_T ranges because of cross p_T range pairs). The larger negative $f^*_{\rm CME}$ is mainly caused by the increased negative effect at high p_T from dijet 3p correlations.

We repeat our analysis of Fig. 5 for peripheral 50–80% collisions. The results are shown in Fig. 8 by the open triangles together with those of the 20– 50% centrality range from Fig. 5. The results in peripheral collisions are systematically shifted towards more negative $f^*_{\rm CME}$ compared to central collisions. This is mainly due to a more significant 3p correlation effect.

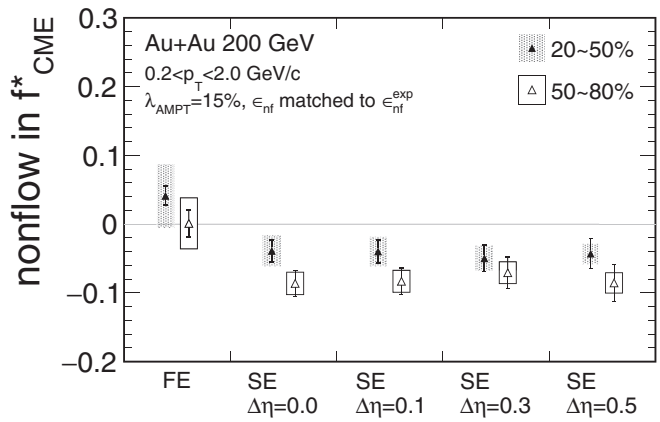

FIG. 8. The nonflow $f^*_{\rm CME}$ estimates in 200 GeV Au+Au collisions for 20–50% centrality (solid triangles, the same as those in Fig. 5) and 50-80% centrality (open triangles).

TABLE I. The STAR SP/PP measurements of $f^*_{\rm CME}$ by the full-event (FE) and subevent (SE) methods [66] together with our estimated nonflow contributions in 20–50% Au+Au collisions at $\sqrt{s_{NN}} = 200$ GeV. The estimates assume charge-dependent 2p correlation effect $\epsilon_2 = 1.7\epsilon_2^{\rm AMPT}$ [59], charge-dependent 3p correlation effect $\epsilon_3 = \epsilon_3^{\rm HIJING} \pm 20\%$ [59], and charge-independent 2p nonflow $\epsilon_{\rm nf}$ by Eq. (23). Two cases of $\epsilon_{\rm nf}$ are tabulated: matched to the experimental data [65] with $\lambda_{\rm AMPT} = 15\%$ (the $\lambda_{\rm AMPT} = 0\%$ results are similar), and not matched to data with $\lambda_{\rm AMPT} = 0\%$ (the $\lambda_{\rm AMPT} = 15\%$ results are similar). The first (or only) quoted error is statistical and the second systematic.

	FE ($p_T = 0.2$–2 GeV/c)	FE ($p_T = 0.2$–1 GeV/c)	SE ($\Delta\eta = 0.1$)	SE ($\Delta\eta = 0.3$)
STAR data	$(14.7 \pm 4.3 \pm 2.6)\%$	$(13.7 \pm 6.2 \pm 2.3)\%$	$(8.8 \pm 4.5 \pm 2.4)\%$	$(6.3 \pm 5.0 \pm 2.5)\%$
$\epsilon_{\rm nf}$ matched to $\epsilon_{\rm nf}^{\rm exp}$, $\lambda_{\rm AMPT} = 15\%$	$(4.1 \pm 1.4 \pm 4.6)\%$	$(6.8 \pm 3.0 \pm 5.5)\%$	$(-4.0 \pm 1.7 \pm 2.1)\%$	$(-5.0 \pm 1.9 \pm 1.8)\%$
$\epsilon_{\rm nf}$ not matched to $\epsilon_{\rm nf}^{\rm exp}$, $\lambda_{\rm AMPT} = 0\%$	$(5.1 \pm 1.7)\%$	$(8.4 \pm 3.6)\%$	$(-4.3 \pm 2.0)\%$	$(-5.6 \pm 2.2)\%$

STAR has measured the $f^*_{\rm CME}$ using the SP/PP method in Au+Au collisions at 200 GeV [66]. We tabulate the STAR measurements together with our estimates of nonflow contributions in Table I. We compare them in Fig. 9 where the STAR data are shown by the red stars and our nonflow estimates are shown by the black triangles. The peripheral collision data are mostly consistent with our nonflow estimates. The central collisions data are systematically larger than our estimations of nonflow contributions (except for the low p_T results). If our nonflow estimations are robust, then the STAR measurements seem to suggest finite CME signals.

VI. SUMMARY AND OUTLOOK

The 3p azimuthal correlator $\Delta\gamma^*$ is dominated by the flow-induced charge-dependent 2p correlation background. The SP/PP method [30] has been proposed to extract the CME signal fraction, $f^*_{\rm CME}$, in the measured $\Delta\gamma^*$ by assuming the background to be proportional to the measured elliptic flow v_2^*. The charge-independent 2p nonflow contamination in v_2^* and the charge-dependent 3p nonflow contribution to $\Delta\gamma^*$ are two further background sources in the extracted $f^*_{\rm CME}$. In this paper we have investigated the effects of these nonflow backgrounds. It is shown that the effects from 2p and 3p nonflow correlations in $f^*_{\rm CME}$ are opposite in sign. They partially cancel each other, making the $f^*_{\rm CME}$ less vulnerable to nonflow. The AMPT and HIJING models are used, together with constraints from experimental data, to quantitatively estimate the magnitudes of those nonflow effects. The main result is given by Eq. (21) and Fig. 5. The main ingredients of our estimation are as follows:

(i) AMPT contains mainly 2p correlations and thus the calculated $f^*_{\rm CME}$ gives a good estimate of the v_2^* nonflow in AMPT, $\epsilon_{\rm nf} = \epsilon_{\rm AMPT}$. The $\epsilon_{\rm nf}$ from AMPT is scaled to match the experimentally deduced nonflow $\epsilon_{\rm nf}^{\rm exp}$ [65]. The residual charge-dependent 3p correlations in AMPT, on the order $\lambda_{\rm AMPT} \approx 15\%$ of those in HIJING [59], have negligible effect in our estimation.

(ii) Charge-dependent 3p correlations ϵ_3 are the main nonflow contribution to $\Delta\gamma^*$. The charge-dependent 3p (dijet) correlations in HIJING, $\epsilon_3^{\rm HIJING}$, are found to give a fair description of the experimental data in small-system collisions ($\epsilon_3 = \epsilon_3^{\rm HIJING} \pm 20\%$) [59]. They are used, together with $\epsilon_2 = 1.7\epsilon_2^{\rm AMPT}$, the flow-induced background $\Delta\gamma_{\rm bkgd}$ in AMPT scaled to match data measurement of $\Delta\gamma^*$, to estimate the 3p nonflow contribution to $f^*_{\rm CME}$.

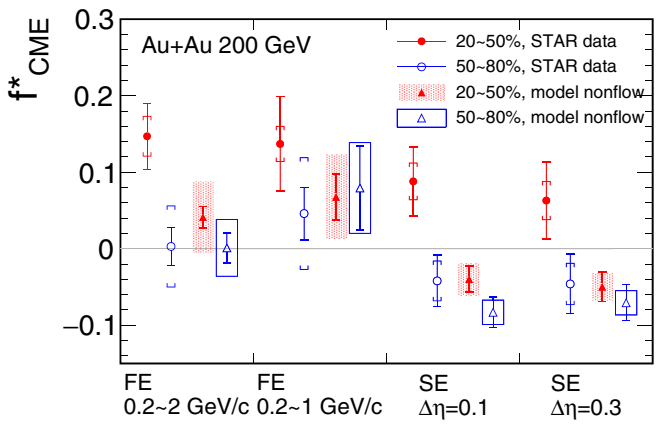

FIG. 9. STAR measurements [66] of $f^*_{\rm CME}$ together with our nonflow estimates within 20–50% (filled markers) and 50–80% (open markers) centralities in 200 GeV Au+Au collisions. The POI and particle c (for EP) are from $|\eta| < 1$ and $0.2 < p_T < 2$ GeV/c except for the second set of points where $0.2 < p_T < 1$ GeV/c. The 2p nonflow effect $\epsilon_{\rm nf}$ is matched to data $\epsilon_{\rm nf}^{\rm exp}$ [65] with $\lambda_{\rm AMPT} = 15\%$, and the 3p nonflow contribution is $\epsilon_3 = \epsilon_3^{\rm HIJING} \pm 20\%$ [59].

It is found, with 2p and 3p nonflow correlations in AMPT and HIJING together with constraints from experimental data, that the nonflow contribution in 20–50% centrality Au+Au collisions at $\sqrt{s_{NN}} = 200$ GeV with the full-event method (without pseudorapidity gap) is approximately $(4 \pm 5)\%$. With the subevent method with pseudorapidity gaps, the nonflow contribution to $f^*_{\rm CME}$ is generally negative, approximately $(-5 \pm 3)\%$. The implications of our nonflow estimates to the STAR measurements are highlighted in Table I and Fig. 9. They suggest that the STAR measurements may imply a finite CME signal.

Further reduction in 2p nonflow contamination in v_2^* by applying larger η gaps, for example, via the forward event-plane detector [67] newly installed in STAR, would be desirable. A forward EP or particle c will, in addition, enable reasonable η gaps to be applied also between the midrapidity α and β particles, reducing the flow-induced background $\Delta\gamma_{\rm bkgd}$ and 3p nonflow contaminations. Future Au+Au runs by STAR with the enhanced forward capability and expected large data volumes would provide definite a conclusion on the CME.

Isobar collision data were collected by STAR in 2018 [68] and a blind data analysis [69] has been carried out. No CME

signatures have been observed by the blind analysis [70]. This may be consistent with a recent estimate using the anomalous-viscous fluid dynamics (AVFD) model, which suggests an effect only on the order of 2σ significance with the collected isobar statistics [71]. Future nonflow studies would be needed in order to quantify or extract an upper limit of the possible CME signal in isobar collisions. The absolute magnitude of the possible CME signal would have large uncertainty, and would require large-volume Au+Au collision data to resolve. Future heavy ion runs by STAR will be important for the CME physics.

It is worthwhile to note that similar magnitudes of the $\Delta\gamma$ variable have been observed at RHIC [10,11] and the LHC [14]. While nonflow background is more diluted by the larger multiplicity at the LHC, more significant resonance/cluster production and larger v_2 have apparently rendered the similar $\Delta\gamma$ magnitude. The SP/PP method has not been applied at the LHC because of limited capability in the first-order event-plane measurements. While one may expect modest increases in 2p and 3p nonflow correlations from RHIC to the LHC, the net effect on the extracted CME fraction, because of their partial cancellation, may be similar between RHIC and the LHC.

ACKNOWLEDGMENTS

We thank Dr. Zi-Wei Lin for providing us the AMPT code with local charge conservation and for discussions. This work is supported by the U.S. Department of Energy (Grant No. DE-SC0012910), the China Hubei Province Department of Education (Grant No. D20201108), the China National Natural Science Foundation (Grants No. 11905059, No. 12035006, No. 12075085, No. 12047568), and the China Ministry of Science and Technology (Grant No. 2020YFE0202001).

[1] T. Lee and G. Wick, Vacuum stability and vacuum excitation in a spin 0 field theory, Phys. Rev. D **9**, 2291 (1974).
[2] P. D. Morley and I. A. Schmidt, Strong P, CP, T violations in heavy ion collisions, Z. Phys. C **26**, 627 (1985).
[3] D. Kharzeev, R. D. Pisarski, and M. H. G. Tytgat, Possibility of Spontaneous Parity Violation in Hot QCD, Phys. Rev. Lett. **81**, 512 (1998).
[4] D. E. Kharzeev, L. D. McLerran, and H. J. Warringa, The Effects of topological charge change in heavy ion collisions: "Event by event P and CP violation", Nucl. Phys. A **803**, 227 (2008).
[5] K. Fukushima, D. E. Kharzeev, and H. J. Warringa, The chiral magnetic effect, Phys. Rev. D **78**, 074033 (2008).
[6] A. Bzdak and V. Skokov, Event-by-event fluctuations of magnetic and electric fields in heavy ion collisions, Phys. Lett. B **710**, 171 (2012).
[7] X.-G. Huang, Electromagnetic fields and anomalous transports in heavy-ion collisions – A pedagogical review, Rep. Prog. Phys. **79**, 076302 (2016).
[8] D. Kharzeev, Parity violation in hot QCD: Why it can happen, and how to look for it, Phys. Lett. B **633**, 260 (2006).
[9] S. A. Voloshin, Parity violation in hot QCD: How to detect it, Phys. Rev. C **70**, 057901 (2004).
[10] B. Abelev *et al.* (STAR Collaboration), Azimuthal Charged-Particle Correlations and Possible Local Strong Parity Violation, Phys. Rev. Lett. **103**, 251601 (2009).
[11] B. Abelev *et al.* (STAR Collaboration), Observation of charge-dependent azimuthal correlations and possible local strong parity violation in heavy ion collisions, Phys. Rev. C **81**, 054908 (2010).
[12] L. Adamczyk *et al.* (STAR Collaboration), Beam-Energy Dependence of Charge Separation Along the Magnetic Field in Au+Au Collisions at RHIC, Phys. Rev. Lett. **113**, 052302 (2014).
[13] L. Adamczyk *et al.* (STAR Collaboration), Fluctuations of charge separation perpendicular to the event plane and local parity violation in $\sqrt{s_{NN}} = 200$ GeV Au+Au collisions at the BNL Relativistic Heavy Ion Collider, Phys. Rev. C **88**, 064911 (2013).
[14] B. Abelev *et al.* (ALICE Collaboration), Charge Separation Relative to the Reaction Plane in Pb-Pb Collisions at $\sqrt{s_{NN}} = 2.76$ TeV, Phys. Rev. Lett. **110**, 012301 (2013).
[15] V. Khachatryan *et al.* (CMS Collaboration), Observation of Charge-Dependent Azimuthal Correlations in p-Pb Collisions and Its Implication for the Search for the Chiral Magnetic Effect, Phys. Rev. Lett. **118**, 122301 (2017).
[16] A. M. Sirunyan *et al.* (CMS Collaboration), Constraints on the chiral magnetic effect using charge-dependent azimuthal correlations in pPb and PbPb collisions at the LHC, Phys. Rev. C **97**, 044912 (2018).
[17] S. Acharya *et al.* (ALICE Collaboration), Constraining the magnitude of the chiral magnetic effect with event shape Engineering in Pb-Pb collisions at $\sqrt{s_{\rm NN}} = 2.76$ TeV, Phys. Lett. B **777**, 151 (2018).
[18] S. Acharya *et al.* (ALICE Collaboration), Constraining the chiral magnetic effect with charge-dependent azimuthal correlations in Pb-Pb collisions at $\sqrt{s_{\rm NN}} = 2.76$ and 5.02 TeV, JHEP 09 (2020) 160.
[19] J. Adam *et al.* (STAR Collaboration), Charge-dependent pair correlations relative to a third particle in p+Au and d+Au collisions at RHIC, Phys. Lett. B **798**, 134975 (2019).
[20] F. Wang, Effects of cluster particle correlations on local parity violation observables, Phys. Rev. C **81**, 064902 (2010).
[21] A. Bzdak, V. Koch, and J. Liao, Remarks on possible local parity violation in heavy ion collisions, Phys. Rev. C **81**, 031901(R) (2010).
[22] S. Schlichting and S. Pratt, Charge conservation at energies available at the BNL Relativistic Heavy Ion Collider and contributions to local parity violation observables, Phys. Rev. C **83**, 014913 (2011).
[23] F. Wang and J. Zhao, Challenges in flow background removal in search for the chiral magnetic effect, Phys. Rev. C **95**, 051901(R) (2017).
[24] J. Zhao and F. Wang, Experimental searches for the chiral magnetic effect in heavy-ion collisions, Prog. Part. Nucl. Phys. **107**, 200 (2019).
[25] J. Schukraft, A. Timmins, and S. A. Voloshin, Ultra-relativistic nuclear collisions: Event shape engineering, Phys. Lett. B **719**, 394 (2013).

[26] L. Adamczyk *et al.* (STAR Collaboration), Measurement of charge multiplicity asymmetry correlations in high-energy nucleus-nucleus collisions at $\sqrt{s_{NN}} = 200$ GeV, Phys. Rev. C **89**, 044908 (2014).

[27] J. Zhao, H. Li, and F. Wang, Isolating backgrounds from the chiral magnetic effect, Eur. Phys. J. C **79**, 168 (2019).

[28] J. Adam *et al.* (STAR Collaboration), Pair invariant mass to isolate background in the search for the chiral magnetic effect in Au+Au collisions at $\sqrt{s_{\rm NN}} = 200$ GeV, arXiv:2006.05035.

[29] H.-j. Xu, X. Wang, H. Li, J. Zhao, Z.-W. Lin, C. Shen, and F. Wang, Importance of Isobar Density Distributions on the Chiral Magnetic Effect Search, Phys. Rev. Lett. **121**, 022301 (2018).

[30] H.-j. Xu, J. Zhao, X. Wang, H. Li, Z.-W. Lin, C. Shen, and F. Wang, Varying the chiral magnetic effect relative to flow in a single nucleus-nucleus collision, Chin. Phys. C **42**, 084103 (2018).

[31] J. Zhao (STAR Collaboration), Measurements of the chiral magnetic effect with background isolation in 200 GeV Au+Au collisions at STAR, in *Proceedings, 27th International Conference on Ultrarelativistic Nucleus-Nucleus Collisions* (Quark Matter 2018), Venice, Italy, May 14–19, 2018 [Nucl. Phys. A **982**, 535 (2019)].

[32] J. Zhao (STAR Collaboration), Search for CME in U+U and Au+Au collisions in STAR with different approaches of handling backgrounds, Nucl. Phys. A **1005**, 121766 (2021).

[33] B. Alver *et al.* (PHOBOS Collaboration), System Size, Energy, Pseudorapidity, and Centrality Dependence of Elliptic Flow, Phys. Rev. Lett. **98**, 242302 (2007).

[34] B. Alver, B. B. Back, M. D. Baker, M. Ballintijn, D. S. Barton, R. R. Betts, R. Bindel, W. Busza, V. Chetluru, E. Garcia, T. Gburek, J. Hamblen, U. Heinz, D. J. Hofman, R. S. Hollis, A. Iordanova, W. Li, C. Loizides, S. Manly, A. C. Mignerey *et al.*, Importance of correlations and fluctuations on the initial source eccentricity in high-energy nucleus-nucleus collisions, Phys. Rev. C **77**, 014906 (2008).

[35] S. Shi and J. Liao (private communication).

[36] J.-Y. Ollitrault, A. M. Poskanzer, and S. A. Voloshin, Effect of flow fluctuations and nonflow on elliptic flow methods, Phys. Rev. C **80**, 014904 (2009).

[37] A. M. Poskanzer and S. A. Voloshin, Methods for analyzing anisotropic flow in relativistic nuclear collisions, Phys. Rev. C **58**, 1671 (1998).

[38] S. Voloshin and Y. Zhang, Flow study in relativistic nuclear collisions by Fourier expansion of Azimuthal particle distributions, Z. Phys. C **70**, 665 (1996).

[39] N. Borghini, P. M. Dinh, and J.-Y. Ollitrault, Are flow measurements at SPS reliable? Phys. Rev. C **62**, 034902 (2000).

[40] N. Borghini, Momentum conservation and correlation analyses in heavy-ion collisions at ultrarelativistic energies, Phys. Rev. C **75**, 021904(R) (2007).

[41] F. Wang, Non-flow correlations in a cluster model, Phys. Rev. C **81**, 064905 (2010).

[42] B. Alver *et al.* (PHOBOS Collaboration), Non-flow correlations and elliptic flow fluctuations in gold-gold collisions at $\sqrt{s_{NN}} =$ 200 GeV, Phys. Rev. C **81**, 034915 (2010).

[43] M. A. Lisa, S. Pratt, R. Soltz, and U. Wiedemann, Femtoscopy in relativistic heavy ion collisions, Annu. Rev. Nucl. Part. Sci. **55**, 357 (2005).

[44] B. Zhang, C. M. Ko, B.-A. Li, and Z. W. Lin, A multiphase transport model for nuclear collisions at RHIC, Phys. Rev. C **61**, 067901 (2000).

[45] Z.-W. Lin, C. M. Ko, B.-A. Li, B. Zhang, and S. Pal, Multiphase transport model for relativistic heavy ion collisions, Phys. Rev. C **72**, 064901 (2005).

[46] X.-N. Wang and M. Gyulassy, HIJING: A Monte Carlo model for multiple jet production in *p*-*p*, *p*-*A*, and *A*-*A* collisions, Phys. Rev. D **44**, 3501 (1991).

[47] M. Gyulassy and X.-N. Wang, HIJING 1.0: A Monte Carlo program for parton and particle production in high-energy hadronic and nuclear collisions, Comput. Phys. Commun. **83**, 307 (1994).

[48] Z.-W. Lin (private communication).

[49] P. Jacobs and X.-N. Wang, Matter in extremis: Ultrarelativistic nuclear collisions at RHIC, Prog. Part. Nucl. Phys. **54**, 443 (2005).

[50] X. Zhang and J. Liao, Event-by-event azimuthal anisotropy of jet quenching in relativistic heavy ion collisions, Phys. Rev. C **87**, 044910 (2013).

[51] R. P. G. Andrade, J. Noronha, and G. S. Denicol, Jet quenching effects on the direct, elliptic, and triangular flow at energies available at the BNL Relativistic Heavy Ion Collider, Phys. Rev. C **90**, 024914 (2014).

[52] G.-Y. Qin, Anisotropic flow and jet quenching in relativistic nuclear collisions, Int. J. Mod. Phys. E **24**, 1530001 (2015).

[53] B. Andersson, G. Gustafson, and B. Soderberg, A general model for jet fragmentation, Z. Phys. C **20**, 317 (1983).

[54] T. Sjöstrand, High-energy physics event generation with PYTHIA 5.7 and JETSET 7.4, Comput. Phys. Commun. **82**, 74 (1994).

[55] T. Sjöstrand, P. Eden, C. Friberg, L. Lonnblad, G. Miu *et al.*, High-energy physics event generation with PYTHIA 6.1, Comput. Phys. Commun. **135**, 238 (2001).

[56] B. I. Abelev *et al.* (STAR Collaboration), Hadronic resonance production in *d*+Au collisions at $\sqrt{s_{NN}} = 200$ GeV at RHIC, Phys. Rev. C **78**, 044906 (2008).

[57] A. Adare *et al.* (PHENIX Collaboration), Transverse energy production and charged-particle multiplicity at midrapidity in various systems from $\sqrt{s_{NN}} = 7.7$ to 200 GeV, Phys. Rev. C **93**, 024901 (2016).

[58] Z.-W. Lin and C. M. Ko, Partonic effects on the elliptic flow at RHIC, Phys. Rev. C **65**, 034904 (2002).

[59] J. Zhao, Y. Feng, H. Li, and F. Wang, HIJING can describe the anisotropy-scaled charge-dependent correlations at the BNL relativistic heavy ion collider, Phys. Rev. C **101**, 034912 (2020).

[60] Z.-W. Lin, Evolution of transverse flow and effective temperatures in the parton phase from a multi-phase transport model, Phys. Rev. C **90**, 014904 (2014).

[61] A. Bzdak and G.-L. Ma, Elliptic and Triangular Flow in *p*+Pb and Peripheral Pb+Pb Collisions from Parton Scatterings, Phys. Rev. Lett. **113**, 252301 (2014).

[62] S. H. Lim, Q. Hu, R. Belmont, K. K. Hill, J. L. Nagle, and D. V. Perepelitsa, Examination of flow and non-flow factorization methods in small collision systems, Phys. Rev. C **100**, 024908 (2019).

[63] J. Adams *et al.* (STAR Collaboration), Identified Particle Distributions in *pp* and Au+Au Collisions at $\sqrt{s_{NN}} = 200$ GeV, Phys. Rev. Lett. **92**, 112301 (2004).

[64] B. Abelev *et al.* (STAR Collaboration), Systematic measurements of identified particle spectra in *pp*, *d*+Au, and Au+Au collisions from STAR, Phys. Rev. C **79**, 034909 (2009).

[65] N. M. Abdelwahab *et al.* (STAR Collaboration), Isolation of

flow and nonflow correlations by two- and four-particle cumulant measurements of azimuthal harmonics in $\sqrt{s_{\rm NN}} = 200$ GeV Au+Au collisions, Phys. Lett. B **745**, 40 (2015).

[66] M. Abdallah *et al.* (STAR Collaboration), Search for the chiral magnetic effect via charge-dependent azimuthal correlations relative to spectator and participant planes in Au+Au collisions at $\sqrt{s_{NN}} = 200$ GeV, arXiv:2106.09243 [Phys. Rev. Lett. (to be published)].

[67] J. Adams *et al.*, The STAR Event Plane Detector, Nucl. Instrum. Methods Phys. Res., Sect. A **968**, 163970 (2020).

[68] V. Koch, S. Schlichting, V. Skokov, P. Sorensen, J. Thomas, S. Voloshin, G. Wang, and H.-U. Yee, Status of the chiral magnetic effect and collisions of isobars, Chin. Phys. C **41**, 072001 (2017).

[69] J. Adam *et al.* (STAR Collaboration), Methods for a blind analysis of isobar data collected by the STAR Collaboration, Nucl. Sci. Tech. **32**, 48 (2021).

[70] M. Abdallah *et al.* (STAR Collaboration), Search for the chiral magnetic effect with isobar collisions at $\sqrt{s_{NN}} = 200$ GeV by the STAR Collaboration at the BNL relativistic heavy ion collider, Phys. Rev. C **105**, 014901 (2022).

[71] Y. Feng, Y. Lin, J. Zhao, and F. Wang, Revisit the chiral magnetic effect expectation in isobaric collisions at the relativistic heavy ion collider, Phys. Lett. B **820**, 136549 (2021).